

*Article*

## Filling-and-Dragging Technique for A Particle-Entrapment Using Triangular Microwells

Phakpoom Yingprathanphon<sup>a</sup>, Tepparit Wongpakham, Werayut Srituravanich, and Alongkorn Pimpin<sup>b,\*</sup>

Department of Mechanical Engineering, Faculty of Engineering, Chulalongkorn University, Bangkok, Thailand

E-mail: <sup>a</sup>phakpoom.y@chula.ac.th, <sup>b</sup>alongkorn.p@chula.ac.th (Corresponding author)

**Abstract.** Trapping particle such as a cell, cell spheroid or scaffold bead, in a large trapping spot, such as a microwell, is important in various biological aspects. To achieve high trapping efficacy, the management of two countering effects from hydrodynamic and gravitational force is a key requirement. To increase the possibility of controllable entrapment, this study proposed a new approach using the filling and dragging technique to trap particles. The investigation of the trapping efficacy in three different shapes of triangular microwells such as obtuse, equilateral and acute triangle was conducted. The extremely low flow rate was firstly introduced to fill the particles in the microwell, and the flow rate was subsequently increased to drag and rearrange the entrapped particles. High trapping rate of a single particle in an array of equilateral triangular microwells could reach 80% when trapping polystyrene beads. For biomaterial particle such as cell spheroids, the adhesiveness with the other and the microwell surface is the parameter that needs to be further investigated.

**Keywords:** Trapping, microwell, bead, cell, microfluidics.

**ENGINEERING JOURNAL** Volume 24 Issue 2

Received 22 August 2019

Accepted 15 January 2020

Published 31 March 2020

Online at <https://engj.org/>

DOI:10.4186/ej.2020.24.2.63

## 1. Introduction

There has been a continuing attempt to study cell to cell interactions to control the growth, function, and differentiation of cells; therefore, various 3D-culture methodologies have been developed recently to support this kind of study. Among them, cell spheroid culture is one of the simplest approaches [1-4], and a formation of 3D cell spheroids using a microwell [2, 4-12] has become a robust and efficient tool to overcome the problems of the conventional methods such as hanging drop and bioreactor techniques.

However, the proliferation of cells in spheroids is still limited by their sizes. Oxygen and nutrients are often inaccessible to cells in the interior of the spheroid aggregates, which can lead to either cell death of the inner cells or differences in behavior between the outer and inner cells.

To resolve the problem, spheroids with biomaterial scaffold particles have been studied [13-17]. This method could provide a suitable surface for cell attachment and space for facile diffusion of nutrients resulting of increasing cell viability and promoting cell proliferation. To facilitate the formation of scaffold/cell spheroids, the microwell is also one of promising techniques used to trap the spherical scaffold beads before loading the cells to attach to the scaffolds [13-15].

Additionally, in some studies, cell spheroids were preformed using other platforms, and then transferred to a trapping spot, such as an array of microwells, inside the culturing chip [18-20]. In these studies, the microfluidic chip was designed to immobilize the cell spheroids and provide suitable microenvironments for further specific biological studies, for example, tissue-tissue interactions and spheroid fusion process.

Therefore, the microwell could be employed to support cell-spheroid researches in several ways, not only for the spheroid formation. However, major drawbacks of the conventional microwell are still remained such as cell loss during operation, non-uniform characteristics depending to microwell size, low trapping rate and high possibility of accumulating of waste surrounding the cells [21-27]. Among many aspects that are needed to be improved, the entrapment with ability to control a number of scaffold-particles or cell-spheroids per a microwell, or in another word, a trapping manner such as single, double or multiple particles/spheroids per a microwell, would be one of the key requirements.

Comparing between different shapes, a triangular microwell is distinctive because it could be specific to single particle/spheroid trapping, and provide a vast space surrounding the entrapped spheroid for the cell growth [28-30].

The triangular microwell has unique flow structures that are hydrodynamically induced from the influence of an asymmetrical shape of the microwell. Figures 1a and 1b show the recirculation inside a triangular microwell

comparing to that in a circular microwell. Briefly, two vortex systems, such as a pair of counter-rotating streamwise vortices and a lateral spanwise vortex, are initiated at the leading edges of the microwell. Consequently, they are interacted to each other resulting of a formation of another pair of streamwise vortices along the vertical side walls inside the microwell. These secondary streamwise vortices could push entrapped particles off the microwell when their strength and spatial extent are adequate. In addition, it has high possibility that a single particle would be trapped at the front corner of the microwell under the influence of the recirculation of spanwise vortex. Apparently, the hydrodynamic force is one factor that has an effect on the motion of particle/spheroid in the microwell.

Another factor is a gravitational force that would have counter effects to the hydrodynamic force. In the case when the gravitational force is extremely stronger, the trapping manner is independent to the flow structures, and particles would fully fill in the microwell regardless of the shape of the microwell. On the other hand, the excessively strong hydrodynamic forces would drag particles along the streamline resulting in low possibility of particle entrapment inside the microwell. Therefore, the management of the magnitude of the two forces becomes a very important issue for the highly effective trapping.

To deal with these countering effects, we propose the new entrapment approach that is divided into two steps as shown in Fig. 2. Firstly, the particles/spheroids are allowed to fully fill in the microwells under the influence of relatively strong gravitational forces at extremely low flow rate condition. After that, the flow rate is increased resulting in the significant increasing of the influence of hydrodynamic force. As a result, entrapped particles/spheroids are selectively dragged out the microwell regarding to the strength and spatial extent of induced flow structures. Using this approach, the trapping process and manner could be easily controlled effectively. With different shapes of microwells, the flow structures as well as the strength of hydrodynamic force should be dissimilar even at the certain flow conditions. As a result, the perturbing formation of settled particles/spheroids should be different depending on the shapes of the microwells.

With respect to the reasons mentioned above, this study aims to employ this two-step trapping approach such as filling and dragging to the different shapes of triangular microwells. Three shapes of microwell such as obtuse, equilateral and acute triangle were employed. At the beginning, computational study was conducted to investigate the effects of the microwell shapes on the formation of flow structures for these three types of microwells. To prove the concept, experimental study with polystyrene beads was then used to examine the trapping efficacy especially for the single-particle manner comparing between all cases. After that, the trapping of cell spheroids was tried using an identical procedure with the polystyrene bead experiments.

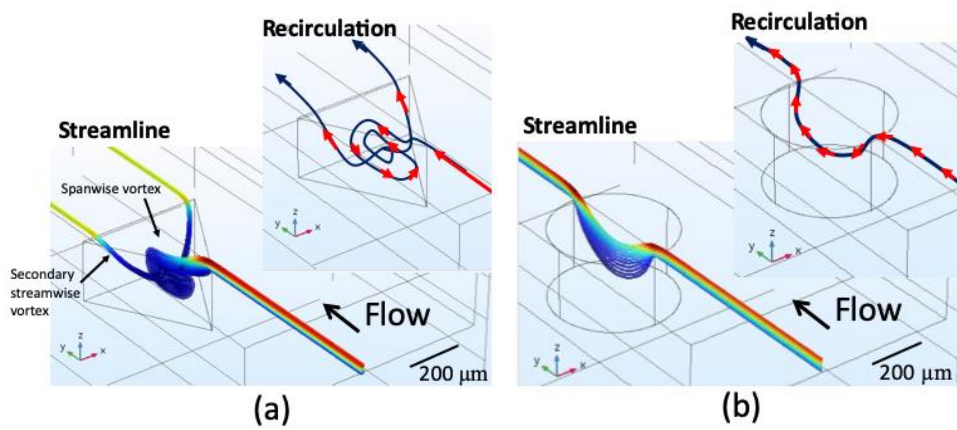


Fig. 1. Flow structures originated from flow streamlines coming in at the middle plane of the (a) triangular, and (b) circular microwells.

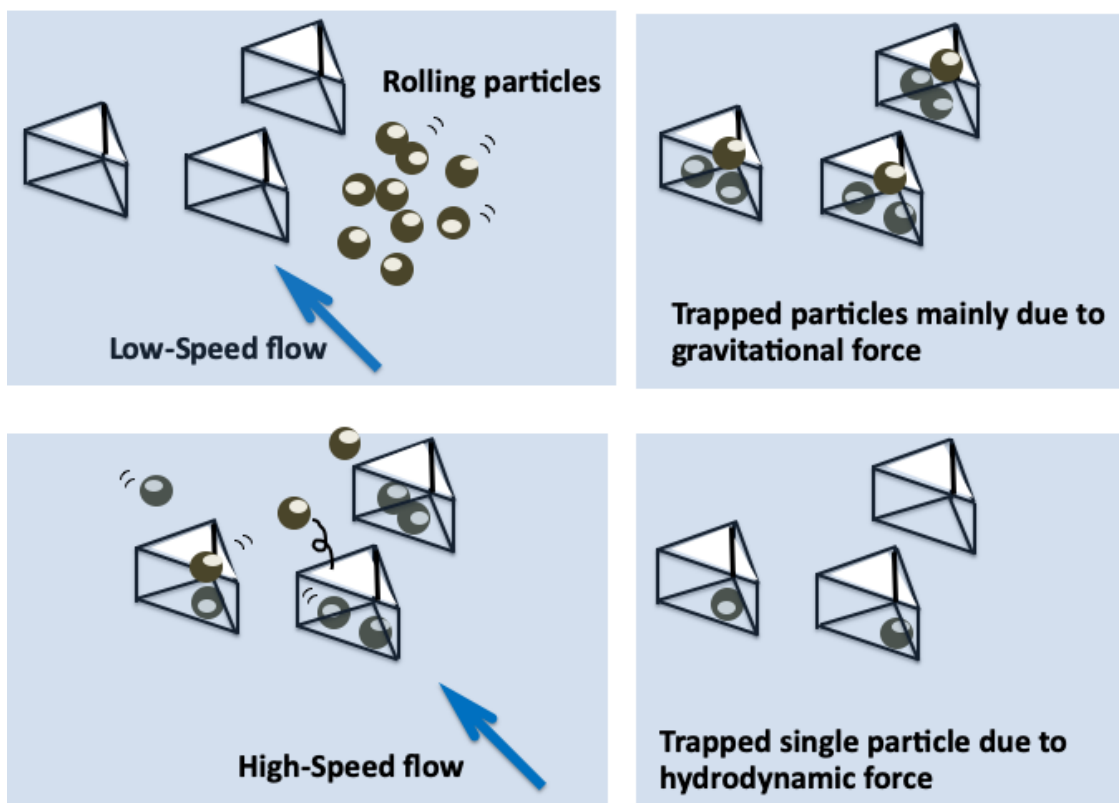


Fig. 2. Filling-and-Dragging technique consecutively using low- and high-speed flow to trap particles in a microwell.

## 2. Flow Simulation

### 2.1. Computational Approach

Three-dimensional simulations were conducted using commercial software, COMSOL Multiphysics®, for the three different shapes of the triangular microwells. Figure 3a shows dimensions of all cases. The working fluid was assumed to be water (a homogeneous, incompressible, Newtonian fluid with density of  $1,000 \text{ kg/m}^3$  and dynamic

viscosity of  $0.001 \text{ Pa}\cdot\text{s}$ ), and the flow was assumed to be laminar and steady. For boundary conditions, a fully developed flow at inlet, a symmetric condition for the side walls, and a no slip condition for the top and bottom of the channel were applied (Fig. 3b). The average flow velocity was  $20 \text{ mm/s}$  that was comparable to that when dragging particles/spheroids in the experiments. Grid-Independence test was performed to ensure the accuracy of computational results. In the study, the simulations for both empty and fully-occupied microwells by  $150 \text{ }\mu\text{m}$  particles were examined.

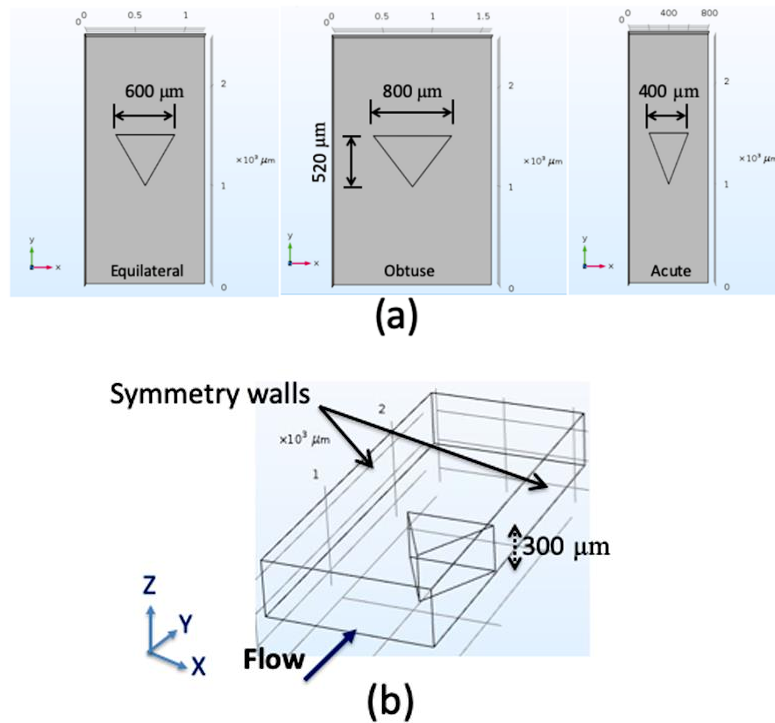


Fig. 3. Computational domains showing (a) microwell sizes for all cases, and (b) applied symmetric-wall condition.

## 2.2. Vorticity Contour

From the simulations, three types of the vortex such as a spanwise vortex, a pair of primary streamwise vortices and a pair of secondary streamwise vortices were clearly observed in the empty microwells. The spanwise vortex is a flow circulation from the back to the front corner of the microwell. In all cases, the spatial extent of the spanwise vortex was comparable, and it had strong influence to the depth of 150-200  $\mu\text{m}$  from the upper plane of the microwell. For the magnitude of vorticity that represents the strength of the flow circulation, the obtuse triangular microwell had relatively strong circulation, which reduced in the equilateral and acute triangular microwell, respectively.

The second vortex system is the pair of the primary streamwise vortices that is initiated at the leading edges of the microwell (see Fig. 4a). They were observed only at the depth less than 100  $\mu\text{m}$  from the upper plane. Beyond that, at the depth between 100 and 250  $\mu\text{m}$  (see Figs. 4b and 4c), another pair of the streamwise vortices, which had the rotation direction opposite to the primary streamwise vortices, was formed due to the interaction between the spanwise vortex and the primary streamwise vortices. Their magnitude as well as spatial extent in the obtuse triangular microwell were relatively large, and reduced for equilateral and acute triangular microwell, respectively. Probably, the strong influence of relatively large confined space inside the obtuse triangular microwell might allow

the progressive evolution of the secondary streamwise vortices.

The comparison of the streamwise vorticity at the frontal and trailing plane for all cases was shown in Figs. 5a and 5b, respectively. Two pairs of the streamwise vortices were clearly observed on both planes. At the frontal plane, the primary streamwise vortices were initiated on the leading edges while the secondary streamwise vortices were formed on the vertical side-walls of the microwell. At the trailing plane, the secondary streamwise vortices became stronger, and moved away from the microwell near the corners at the back of the microwell.

With the entrapped particles of 150  $\mu\text{m}$ , the spanwise vortex and primary streamwise vortices still penetrated to the same depth with that observed in the empty microwells. The secondary streamwise vortices were observed as well. In the obtuse and equilateral triangular microwells, their magnitude as well as spatial extent were larger comparing to that in the empty microwells of the same shape (see example for the equilateral triangular microwell in Fig. 6). Except in the acute triangular microwell, no significant change was observed. For these cases, the confined space got smaller as the depth between the spanwise vortex at the top and entrapped particles at the bottom reduced to 150  $\mu\text{m}$ . This reduction of the confined space might increase the relatively strong interaction between the flow structures and the entrapped particles in the obtuse and equilateral triangular microwells.

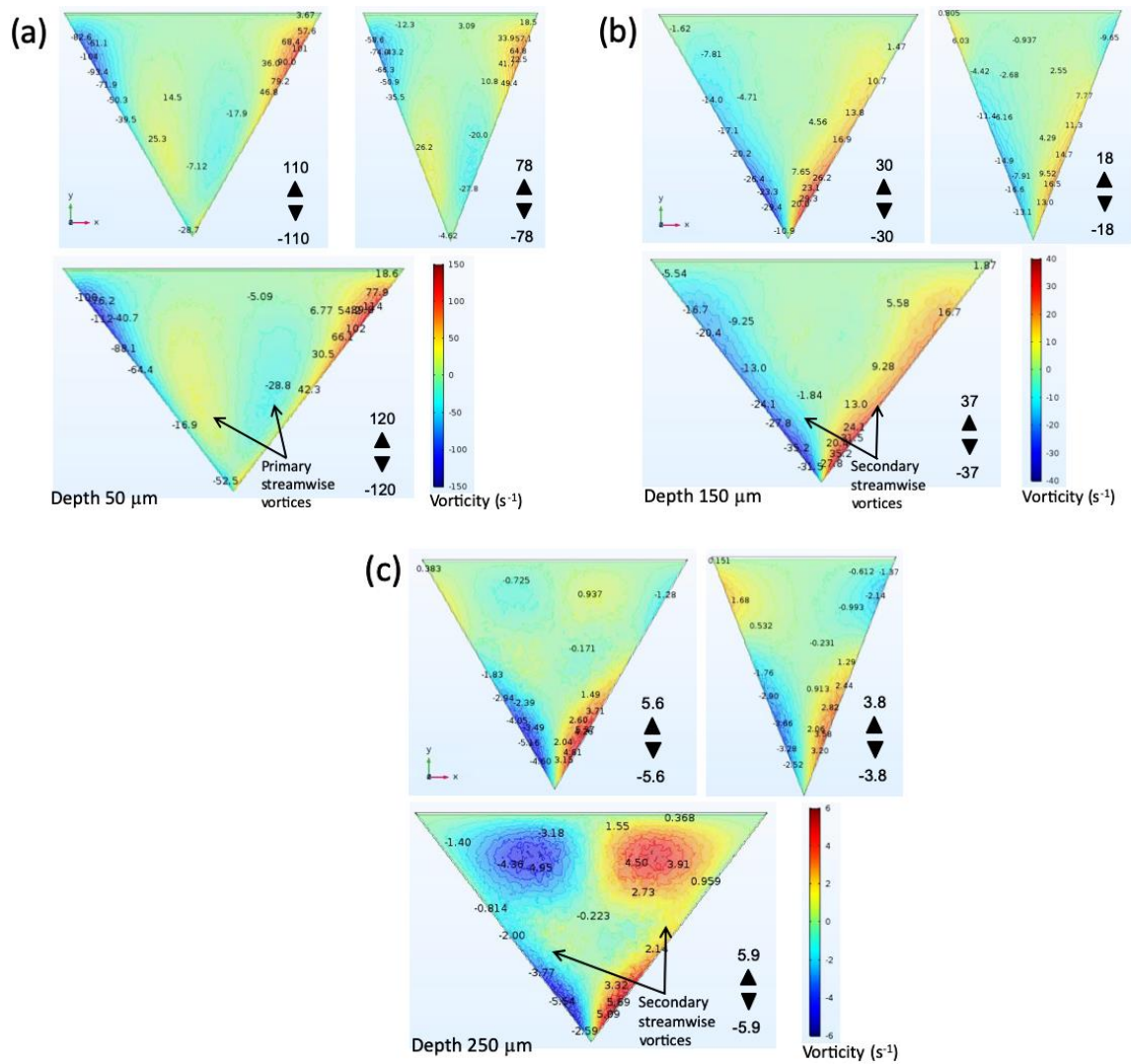


Fig. 4. Streamwise vorticity for all cases on the plane of (a) 50, (b) 150, and (c) 250  $\mu\text{m}$  below the upper plane of the empty microwells.

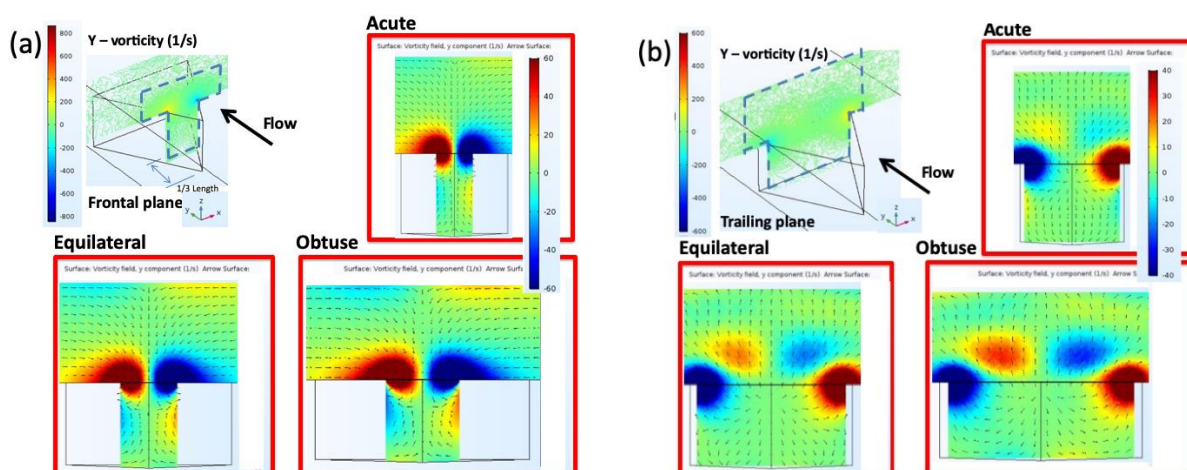


Fig. 5. Streamwise vorticity for all cases on the (a) frontal, and (b) trailing plane in the empty microwells.

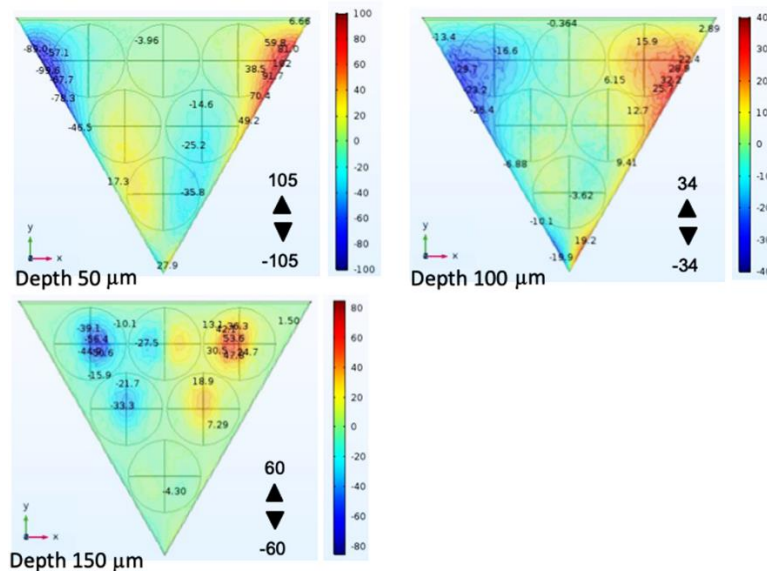


Fig. 6. Streamwise vorticity on the plane of (a) 50, (b) 100, and (c) 150  $\mu\text{m}$  below the upper plane of the equilateral microwell, which was fully filled with 150  $\mu\text{m}$  particles.

### 2.3. Surface-Averaged Vorticity

Surface-averaged vorticity in the streamwise direction on the plane deeper in the microwells was calculated for all cases. It represents the strength of flow circulation. If the strength is adequate, the flow circulation might perturb and pull entrapped particles along.

For the empty microwell shown in Fig. 7a, the averaged vorticity in the streamwise direction for all cases decreased from the upper to the lower plane. Among all cases, the magnitude of averaged streamwise vorticity of the acute triangular microwell was weaker than the other cases. Except at the depth of 250  $\mu\text{m}$ , the difference of the magnitude of averaged streamwise vorticity of all cases significantly reduced probably due to the influence of the bottom wall of the microwell.

In the case of microwells with entrapped particles as shown Fig. 7b, at the depth of 100-150  $\mu\text{m}$ , or the plane above the entrapped particles, the tendency of the averaged streamwise vorticity in the acute triangular microwell was similar to the empty microwell. It was probably due to the relatively weak interaction between the spanwise and primary streamwise vortices, especially inside the microwell. Therefore, the small confined space, when the microwell was occupied, had no significant effect to change the flow structures. On the other hand, the averaged vorticity in the obtuse triangular microwell happened to increase beyond the middle plane at the location close to the entrapped particles. Besides, its magnitude became considerably higher than the other cases. This implied that the interaction between the spanwise and primary streamwise vortices of this case was undoubtedly enhanced further, resulting of the strong secondary streamwise vortices that possibly perturbed the entrapped particles much impactfully.

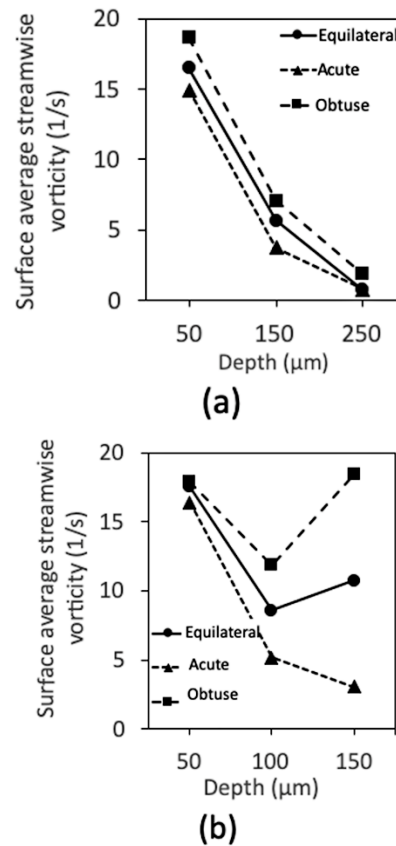


Fig. 7. Surface-averaged streamwise vorticity at different depths for all cases when (a) the microwell was empty, and (b) fully filled with 150- $\mu\text{m}$  particles.

### 2.4. Flow Region

From the results, it could be divided the induced flow into two flow regions such as at the upper region, the plane at the depth between 0-100  $\mu\text{m}$ , and the lower region, the plane at the depth between 100-150  $\mu\text{m}$  and beyond. In the first region, the vorticities represent the existence

of the primary streamwise vortices. The results implied that, in the equilateral and obtuse triangular microwells, the primary streamwise vortices had stronger influence deeper into the microwell, when comparing to the acute triangular case.

In the second region, the vorticities represent the existence of the secondary streamwise vortices, and the magnitude of averaged vorticity should be related to the evolution of the vortices as mentioned earlier. With the wider space in the obtuse triangular microwell, the growth of secondary streamwise vortices could be occurred with less constraint resulting to the higher averaged vorticities. Despite of that, at the plane beyond 150  $\mu\text{m}$ , the averaged vorticities were drastically low in all cases. It implied that the influence of the freestream flow above the microwell was only existed within a certain depth, around 150  $\mu\text{m}$  in these cases.

In summary, the effects of the flow circulation that could alter the arrangement of settled particles should depend on the shape of the microwells. In the acute triangular microwell, the formation of secondary streamwise vortices was limited so that their strength was weaker comparing to the other cases. Because of that, it is possible that the influence of hydrodynamics forces would be too little in the acute triangular microwell, and the flow might be unable to pull entrapped particles along. When the confined space became larger, the strength of secondary streamwise vortices was increased, and became stronger for the equilateral and obtuse triangular microwell, respectively. However, it is possible that the flow perturbation might be too strong, over the level that all entrapped particles could persist, and all of them would flow along the streamlines out of the microwells. Furthermore, on the plane deeper than a half of the microwell depth, or about 150  $\mu\text{m}$ , the strength of the flow circulation became very small. As a result, the influence of the flow circulation might be too weak to alter the motion of the particles located lower than that depth in the microwell.

### 3. Two-Step Trapping

#### 3.1. Experimental Setup

To prove the concept of the new trapping approach, the experiments with polystyrene beads of 150  $\mu\text{m}$  (purchased from Sigma-Aldrich), which was equivalent to the diameter of desired particle/spheroid, were conducted. In experiments, the microwells with the similar dimensions (300  $\mu\text{m}$  deep, 520  $\mu\text{m}$  long and 400, 600 and 800  $\mu\text{m}$  wide, respectively, for an acute, equilateral and obtuse triangular microwell) to those in the simulation were employed. The microfluidic chip was made of polydimethylsiloxane (PDMS) using a standard soft lithography. It consisted of a low-aspect-ratio rectangular chamber with the dimensions of 12.5 x 22 x 0.35  $\text{mm}^3$ , in which an array of microwells (the number of wells about 250, 210, 170, respectively, for acute, equilateral and obtuse triangular microwell) were placed at the bottom of

the chamber as shown in Fig. 8a. The distance between each microwell, about 500-600  $\mu\text{m}$ , was long enough as the effects of the recirculation in the upstream microwell on the flow in the following downstream microwell were little. The experimental setup consisted of a microscope, VDO camera and a suction syringe pump.

In experiments, the concentration of polystyrene beads in phosphate buffered saline (PBS) solution was prepared at 1,200-1,500 beads/ml. At the beginning, the microfluidic chip was fully filled with PBS solution, and air bubbles inside were completely removed. Three milliliters of polystyrene beads/PBS solution was fed into the microfluidic chip with the flow rate of 10 ml/hr for 15 minutes to fill up beads inside the microwells. After that, the pure PBS solution with the flow rate of 500 ml/hr was fed to drag entrapped beads out from the microwells for 2 minutes. Figure 8b shows the consecutive images captured from the experiments.

#### 3.2. Experiments with Polystyrene Beads

To quantify the trapping efficacy, the photographing technique was employed to capture the images of occupied microwells at the middle of the microwells. Each image contains about 65, 55 and 45 microwells, respectively, for an acute, equilateral and obtuse triangular microwell. It was about 25% of total number of the microwells that were examined in each case. From the captured images, the number of entrapped beads inside those microwells was counted, and the results were reported as a number of the microwells which entrapped beads for a single, double, or more at that time. Independent experiments for each case were repeated 5 times ( $n=5$ ).

When the dragging process using the higher flow rate starts, the particles are dragged out, and the number of entrapped particles would reduce. The appearance of the double and single entrapment would increase gradually. Because of the difference in dimension, the number of entrapped particles could be accommodated inside each type of the microwell is different. As the number of the particles at the beginning for the acute is less, only three particles, the appearance of the two entrapped particles would be observed earlier comparing to the other cases. For all cases, the empty microwell would happen if all particles are dragged out when the strong perturbation due to the flow circulation is introduced.

From the experimental results (Figs. 9 a-c), the number of multiple entrapped particles sharply reduced within 15-30 s for all cases. It implied that the flow circulation inside the microwells with the flow rate of 500 ml/hr was adequate to suddenly perturb the settled particles and pull them along.

For the equilateral triangular microwell shown in Fig. 9a, the single entrapment increased to and remained at 80%. The double entrapment was not observed while the increment rate of the number of empty microwells was fast. It implied that the influence of the flow perturbation was adequate, and resulted to the short appearance of the

double entrapment. On the other word, the transition from multiple to single entrapment was relatively quick. Fortunately, the perturbation was not strong enough to pull the single particle entrapped at the front corner out from the microwell.

Interestingly, the number of occupied microwells with the multiple particles was remained about 40% for the acute triangular case even it slightly reduced afterwards as shown in Fig. 9b. In addition, the number of both single

and double entrapment increased to 30% and remained at that level while the empty microwell gradually appeared when the time passed by. The relatively weak perturbation due to the flow circulation for the acute triangular microwell comparing to the equilateral microwell would cause this slow transition of the particle arrangement to be happened.

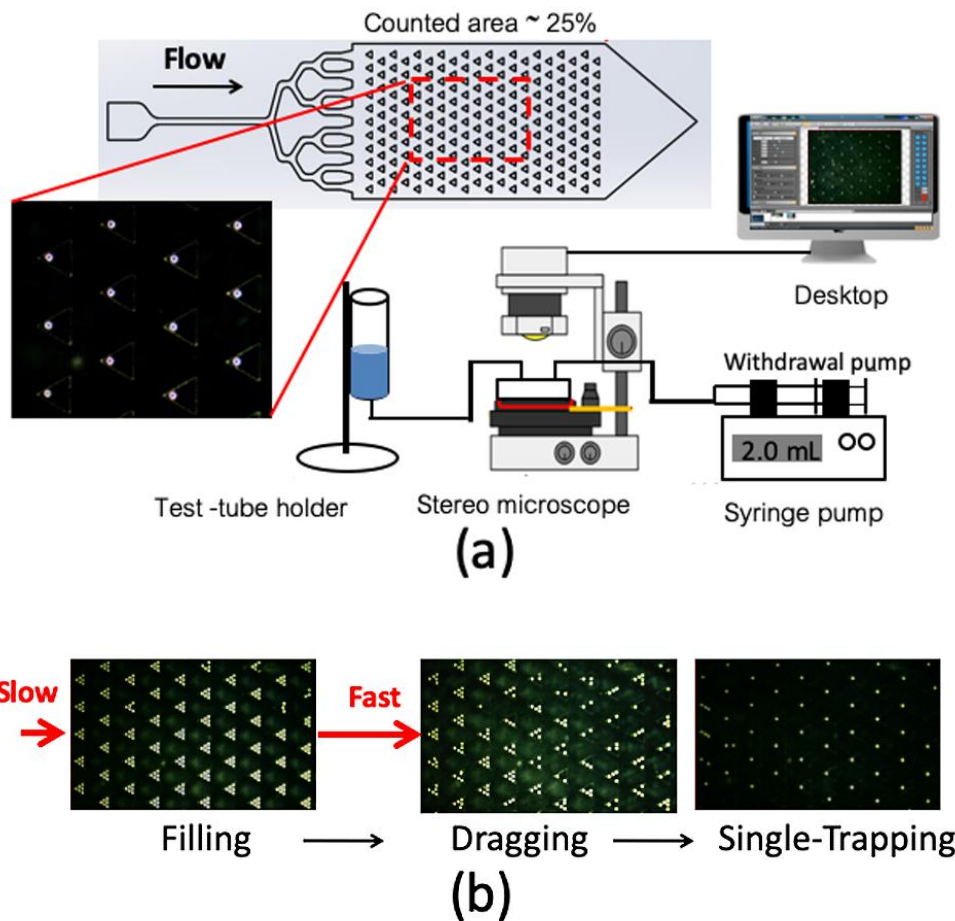


Fig. 8. Experimental setup showing (a) the array of microwells and setup arrangement, and (b) time-lapsed images for the polystyrene-bead trapping.

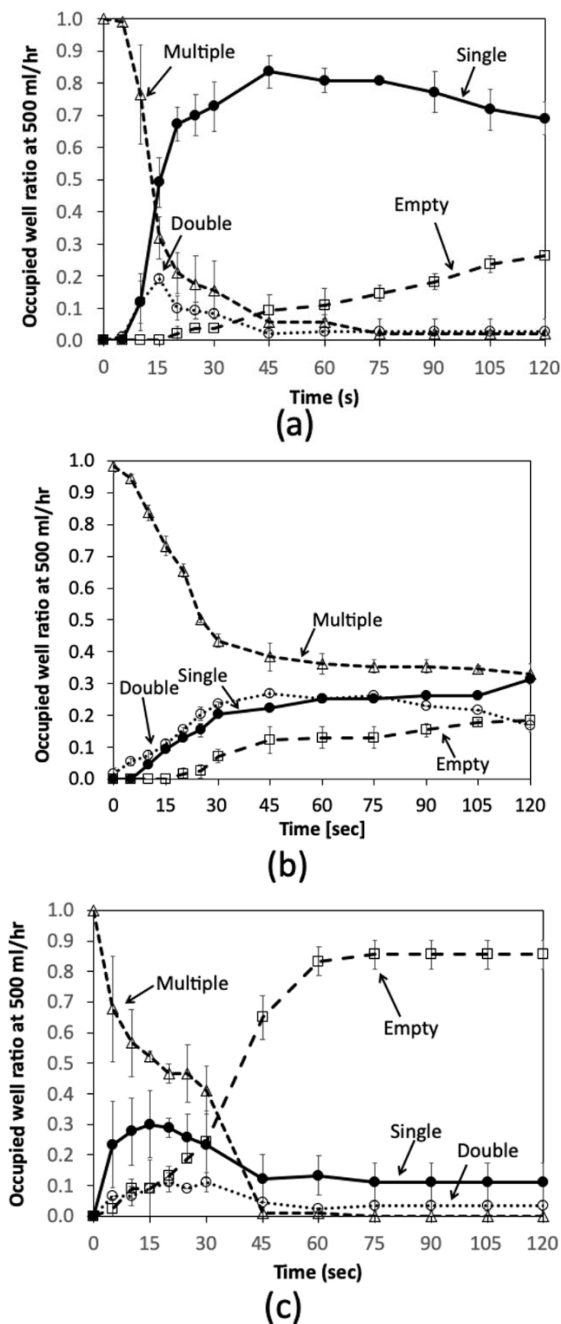


Fig. 9. Ratio of the number of occupied microwells with 150  $\mu\text{m}$  polystyrene beads to all ones, when the dragging with the flow rate of 500 ml/hr was applied. The results are for the (a) equilateral, (b) acute, and (c) obtuse triangular microwells, respectively. The average was taken from 5 independent tests.

For the obtuse triangular microwells shown in Fig. 9c, the empty microwells quickly appeared comparing to the other cases. The transition from the different trapping manner was very quick as the appearance of single and double entrapments was little. This might be happened due to the relatively strong flow perturbation induced in this case as explained in the simulation section.

Therefore, the experimental results with polystyrene beads suggested that the equilateral triangular microwell

was the most appropriate among three different shapes in this study as the flow perturbation was adequate. As a result, the particle trapping could be effectively controlled, and the possibility of single entrapment could reach 80%.

### 3.3. Experiments with Cell Spheroids

The experiments were set up trying to use an identical protocol, such as spheroid concentration in buffer solution and flow rates, with that in the previous section. For the spheroid preparation, mouse embryonic stem cells were cultured on mitomycin C-inactivated confluent mouse embryonic fibroblast (MEF) feeder layers. These cells were maintained in ES medium consisting of Dulbecco's modified Eagle medium (DMEM, HyClone) supplemented with 10% fetal bovine serum (FBS; ES grade, gibco, USA), 5 ng/ml mouse leukemia inhibitory factor (LIF; Merck, USA), 0.1 mM  $\beta$ -mercaptoethanol ( $\beta$ -ME), 0.1 mM nonessential amino acids (NEAA), 1% glutamine and 1% antibiotic-antimycotic solution. The mouse embryonic stem cells were cultured on feeder layers for at least two passages after thawing and prior to the differentiation procedure. After that, the cells were then transferred and cultured for at least one passage in feeder-free conditions on Matrigel matrix-coated plates with LIF in the ES medium. To maintain the culture conditions, the embryonic stem cells were transferred to fresh medium every 1–2 days prior to reaching 70% confluency. The cell culture reagents were purchased from Invitrogen Life Technologies (Grand Island, NY, USA), and all chemicals were purchased from Sigma-Aldrich (St Louis, MO, USA).

After the embryonic stem cells were cultured and grown up to 70% confluence, whereupon monolayers were rinsed twice with PBS solution. After draining well, 2 ml of 0.05% trypsin-1 mM EDTA was added (for 60 mm plates) for 2 min until the cells detached. Trypsinization was stopped by adding 2 ml of complete medium and gently used a 5 ml pipette to triturate the mixture until the cells were in suspension. The cells were transferred to a 15 ml conical tube. After that, cell suspension was centrifuge at 1000 rpm for 5 minutes. Then, the supernatant was discarded and washed pellet with 1 ml differentiation medium (Embryoid Body medium or EB medium like ES medium except FBS and without LIF, FBS defined from Hyclone, GE Healthcare Life Sciences, USA). The cells suspension was resuspended again in 2 ml of EB medium. The cells were count using a hemocytometer and adjusted the concentration to  $2.5 \times 10^4$  cells/ml (500 cells in 20  $\mu\text{l}$ /drop).

The 5 ml of PBS solution was placed into the bottom of 100 mm bacterial dish. This was act as a hydration chamber. The lid of the bacterial dish was inverted then the 20  $\mu\text{l}$  of prepared cell suspension was dropped on the lid with sufficiently apart so as to not touch each other. It was possible to place at least 100 drops per dish. After that, the lid was closed onto the PBS-filled bottom chamber and incubated at 37°C/5% CO<sub>2</sub>/95% humidity. The

drops were monitored daily and incubated for embryoid body formation (approximately one day). The inverted light microscope was used to investigate during the embryoid body formation as an example in Fig. 10a. The diameter of cell spheroids was in the range between 150 and 200  $\mu\text{m}$ .

Then, the experiments to entrap the cell spheroids were started using the identical procedure in the experiments with polystyrene beads, and the images of entrapped cell spheroids in the equilateral triangular microwell are shown in Fig. 10 b. We found that most cell spheroids attached to the others and remained in the microwells even increasing the flow rate from 500 to 700

ml/hr. The single spheroid trapping was hardly occurred. It implied that the cell properties such as membrane adhesiveness play an important role to the achievement of the proposed approach as well as the possibility for single spheroid entrapment. The higher flow rate to drag cell spheroids was also tried. At the flow rate of 900 ml/hr, more cell spheroids oscillated due to the strong flow perturbation. However, some cells started to detach from the broken cell spheroids due to the shear stresses of the freestream flow. Similar issues occurred in the experiments with gelatin beads as they well adsorbed to the PDMS surface, and it was difficult to drag them out from the microwell.

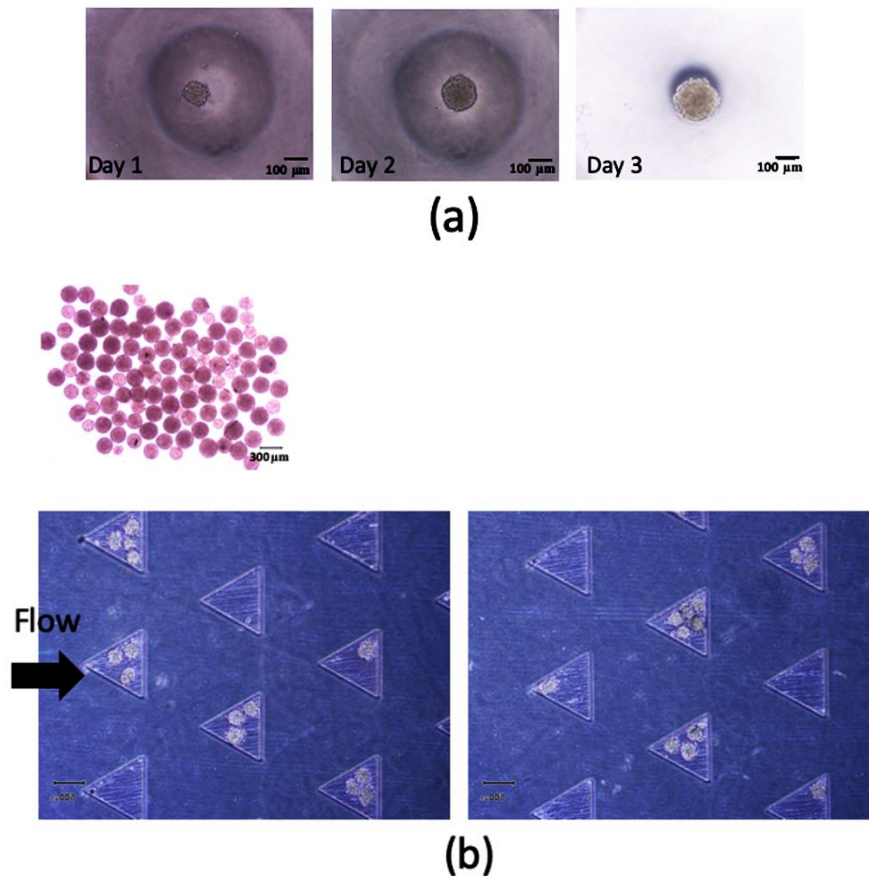


Fig. 10. Captured images from the experiments with cell spheroids showing (a) the formation of cell spheroid for three days using a hanging-drop technique, and (b) entrapped cell spheroids in the equilateral triangular microwells.

#### 4. Conclusions

This study proposed the filling and dragging technique that could lead to high trapping efficacy of particles in a microwell. Using extremely low flow rate at the beginning, it allowed particles to be fully entrapped in the microwell. Then, the significant increasing of the flow rate to drag some entrapped particles out was consecutively conducted. This could lead to a reduction of the number of entrapped particles in the microwell. In this study, three different shapes of the triangular microwells; obtuse, equilateral and acute triangle, were examined for their influence on the trapping efficacy. All microwells had

a length of 520  $\mu\text{m}$  and a depth of 300  $\mu\text{m}$ . The obtuse, equilateral and acute triangular microwell had a hypotenuse length of 800, 600 and 400  $\mu\text{m}$ , respectively. The flow simulation suggested that the microwell shape should have different effects on the flow characteristics. For example, strong interaction between the flow structures and the flow structure-entrapped particles could be found in the obtuse triangular microwell while that of the acute triangular microwell was weak. In the experiments, 150  $\mu\text{m}$  polystyrene beads were employed at two flow rates such as 10 and 500 ml/hr for the filling and dragging, respectively. Comparing between three cases, the polystyrene beads in the acute triangular microwells

were rarely and slowly dragged out, while that in the obtuse ones was very quick comparing to the other cases. The experimental results with polystyrene beads suggested that the equilateral triangular microwell was the most appropriate among three different shapes as the flow perturbation was adequate, and the trapping manner was fairly controllable. It was found that the trapping of a single bead could reach 80%. Lastly, the identical procedures were introduced to the cell spheroids with the comparable diameter. The rearrangement of the cell spheroids in the microwells was rarely observed as the cells attached to each other and adsorbed to the microwells. Instead, the cells started detach from the spheroid when the flow rate was increased beyond 900 ml/hr. At present, this proposed technique has already shown its suitability for plastic or metal particle trapping; however, the further investigation for the trapping of biomaterial particle is needed.

### Acknowledgement

This work was a part of the intelligent 3D printing for development project, financially supported by the Chulalongkorn Academic Advancement into Its 2nd Century Project. In addition, the authors would like to sincerely thank Sudchaya Bhanpattanakul, Thammawit Suwannaphan and Theerawat Tharasanit for their assistance on cell-spheroid experiments.

### References

- [1] E. Fennema, N. Rivron, J. Rouwkema, C. van Blitterswijk, and J. de Boer, "Spheroid culture as a tool for creating 3D complex tissues," *Trends in Biotechnology*, vol. 31, no.2, pp. 108-115, 2013.
- [2] Y. S. Hwang, J. Kim, H. J. Yoon, J. I. Kang, K. H. Park, and H. Bae, "Microwell-Mediated cell spheroid formation and its applications," *Macromol. Res.*, vol. 26, no. 1, pp.1-8, 2017.
- [3] M. W. Laschke and M. D. Menger, "Life is 3D: Boosting spheroid function for tissue engineering," *Trends in Biotechnology*, vol. 35, no. 2, pp. 133-144, 2017.
- [4] K. Moshksayan, N. Kashaninejad, M. E. Warkiani, J. G. Lock, H. Moghadas, B. Firoozabadi, M. S. Saidi, and N.T. Nguyen, "Spheroids-on-a-chip: Recent advances and design considerations in microfluidic platforms for spheroid formation and culture," *Sensors Actuators B*, vol. 263, pp. 151-176, 2018.
- [5] S. Lindström, M. Eriksson, T. Vazin, J. Sandberg, J. Lundeberg, J. Frisén, and H. Andersson-Svahn, "High-density microwell chip for culture and analysis of stem cells," *PLOS ONE*, vol. 4, no. 9, p. e6997, 2009.
- [6] L. Liu, C. Luo, X. Ni, L. Wang, K. Yamauchi, S. Nomura, N. Nakatsuji, and Y. Chen, "A micro-channel-well system for culture and differentiation of embryonic stem cells on different types of substrate," *Biomed Microdevices*, vol. 12, pp. 505-511, 2010.
- [7] S. H. Hsu, Y. H. Ni, and Y. C. Lee, "Microwell chips for selection of bio-macromolecules that increase the differentiation capacities of mesenchymal stem cells," *Macromolecular Bioscience*, vol. 13, pp. 1100-1109, 2013.
- [8] G. Pettinato, X. Wen, and N. Zhang, "Formation of well-defined embryoid bodies from dissociated human induced pluripotent stem cells using microfabricated cell-repellent microwell arrays," *Scientific Reports*, vol. 4, article no. 7402, 2014.
- [9] X. Gong, C. Lin, J. Cheng, J. Su, H. Zhao, T. Liu, X. Wen, and P. Zhao, "Generation of multicellular tumor spheroids with microwell-based agarose scaffolds for drug test," *PLOS ONE*, vol. 10, no. 6, p. e0130348, 2014.
- [10] I. Lilge, S. Jiang, and H. Schönherr, "Long-term stable poly(acrylamide) brush modified transparent microwells for cell attachment studies in 3D," *Macromolecular Bioscience*, vol. 17, p. 1600451, 2017.
- [11] M. Marimuthu, N. Rousset, A. St-Georges-Robillard, M. A. Lateef, M. Ferland, A. M. Mes-Masson, and T. Gervais, "Multi-Size spheroid formation using microfluidic funnels," *Lab Chip*, vol. 18, pp. 304-314, 2018.
- [12] T. Deckers, T. Lambrechts, S. Viazzi, G. N. Hall, I. Papantoniou, V. Bloemen, and J. M. Aerts, "High-throughput image-based monitoring of cell aggregation and microspheroid formation," *PLOS ONE*, vol. 13, no. 6, p. e0199092, 2018.
- [13] W. Leong, A. Kremer, and D. A. Wang, "Development of size-customized hepatocarcinoma spheroids as a potential drug testing platform using a sacrificial gelatin microsphere system," *Materials Science and Engineering C*, vol. 63, pp. 644-49, 2016.
- [14] S. Cocoltan, I. C. Stancu, D. M. Dragusin, A. Serafim, A. Lungu, C. Tucureanu, I. Caras, V. C. Tofan, A. Salageanu, E. Vasile, R. Mallet, D. Chappard, C. Coman, M. Istodorescu, and H. Iovu, "Nanocomposite particles with improved microstructure for 3D culture systems and bone regeneration," *J Mater Sci: Mater Med*, vol. 28, no. 10, p. 153, 2017.
- [15] Y. Kim, P. Baipaywad, Y. Jeong, and H. Park, "Incorporation of gelatin microparticles on the formation of adipose-derived stem cell spheroids," *Int. J. Biological Macromolecules*, vol. 110, pp. 472-478, 2018.
- [16] W. Leong and D. A. Wang, "Cell-laden polymeric microspheres for biomedical applications," *Trends in Biotechnology*, vol. 33, no. 11, pp. 653-66, 2015.
- [17] X. Yue, T. D. Nguyen, V. Zellmer, S. Zhang, and P. Zorlutuna, "Stromal cell-laden 3D hydrogel microwell arrays as tumor microenvironment model for studying stiffness dependent stromal cell-cancer interactions," *Biomaterials*, vol. 170, pp. 37-48, 2018.
- [18] J. Y. Kim, D. A. Fluri, R. Marchan, K. Boonen, S. Mohanty, P. Singh, S. Hammad, B. Landuyt, J. G. Hengstler, J. M. Kelm, A. Hierlemann, and O. Frey, "3D spherical microtissues and microfluidic

- technology for multi-tissue experiments and analysis,” *J. Biotechnology*, vol. 205, pp. 24-35, 2015.
- [19] A. Munaz, R. K. Vadivelu, J. A. St-John, and N. T. Nguyen, “A lab-on-a-chip device for investigating the fusion process of olfactory ensheathing cell spheroids,” *Lab Chip*, vol. 16, no. 15, pp. 2946-2954, 2016.
- [20] A. R. Aref, M. Campisi, E. Ivanova, A. Portell, D. Larios, B. P. Piel, N. Mathur, C. Zhou, R. V. Coakley, A. Bartels, M. Bowden, Z. Herbert, S. Hill, S. Gilhooley, J. Carter, I. Canadas, T. C. Thai, S. Kitajima, V. Chiono, C. P. Paweletz, D. A. Barbie, R. D. Kamm, and R. W. Jenkins, “3D microfluidic ex vivo culture of organotypic tumor spheroids to model immune checkpoint blockade,” *Lab Chip*, vol. 18, no. 20, pp. 3129-3143, 2018.
- [21] Y. Sakai, S. Yoshida, Y. Yoshiura, R. Mori, T. Tamura, K. Yahiro, H. Mori, Y. Kanemura, M. Yamasaki, and K. Nakazawa, “Effect of microwell chip structure on cell microsphere production of various animal cells,” *J. Bioscience Bioengineering*, vol. 110, no. 2, pp. 223-29, 2010.
- [22] K. Nakazawa, Y. Yoshiura, H. Koga, and Y. Sakai, “Characterization of mouse embryoid bodies cultured on microwell chips with different well sizes,” *J. Bioscience Bioengineering*, vol. 116, no. 5, pp. 628-33, 2013.
- [23] K. Futrega, J. S. Palmer, M. Kinney, W. B. Lott, M. D. Ungrin, P. W. Zandstra, and M. R. Doran, “The microwell-mesh: A novel device and protocol for the high throughput manufacturing of cartilage microtissues,” *Biomaterials*, vol. 62, pp. 1-12, 2015.
- [24] J. M. Cha, H. Park, E. K. Shin, J. H. Sung, O. Kim, W. Jung, O. Y. Bang, and J. Kim, “A novel cylindrical microwell featuring inverted-pyramidal opening for efficient cell spheroid formation without cell loss,” *Biofabrication*, vol. 9, p. 035006, 2017.
- [25] G. H. Lee, J. S. Lee, G. H. Lee, W. Y. Joung, S. H. Kim, S. H. Lee, J. Y. Park, and D. H. Kim, “Networked concave microwell arrays for constructing 3D cell spheroids,” *Biofabrication*, vol. 10, no. 1, p. 015001, 2018.
- [26] L. D. Ma, Y. T. Wang, J. R. Wang, J. L. Wu, X. S. Meng, P. Hu, X. Mu, Q. L. Liang, and G. A. Luo, “Design and fabrication of a liver-on-a-chip platform for convenient, highly efficient, and safe in situ perfusion culture of 3D hepatic spheroids,” *Lab Chip*, vol. 18, no. 17, pp. 2547-2562, 2018.
- [27] A. Seyfoori, E. Samiei, N. Jalili, B. Godau, M. Rahmanian, L. Farahmand, K. Majidzadeh-A and M. Akbari, “Self-filling microwell arrays (SFMA) for tumor spheroid formation,” *Lab Chip*, vol. 18, no. 22, pp. 3516-3528, 2018.
- [28] J. Y. Park, M. Morgan, A. N. Sachs, J. Samorezov, R. Teller, Y. Shen, K. J. Pienta, and S. Takayama, “Single cell trapping in larger microwells capable of supporting cell spreading and proliferation,” *Microfluid Nanofluid*, vol. 8, pp. 263–268, 2010.
- [29] C. Tu, B. Huang, J. Zhou, Y. Liang, J. Tian, L. Ji, X. Liang, and Z. Ye, “A microfluidic chip for cell patterning utilizing paired microwells and protein patterns,” *Micromachines*, vol. 8, no. 1, 2017. doi:10.3390/mi8010001
- [30] A. Hattori, T. Yagi, and C. W. Tsao, “Encapsulation of single cells into fixed droplets using triangular microwells,” *Electronics Communications in Japan*, vol. 99, no. 2, pp. 55-63, 2016.

**Phakpoom Yingprathanphon**, photograph and biography not available at the time of publication.

**Tepparit Wongpakham**, photograph and biography not available at the time of publication.

**Werayut Srituravanich**, photograph and biography not available at the time of publication.

**Alongkorn Pimpin**, photograph and biography not available at the time of publication.